

Document downloaded from:

<http://hdl.handle.net/10251/51768>

This paper must be cited as:

Berenguer Betrián, R.; Sieben, JM.; Quijada Tomás, C.; Morallón, E. (2014). Pt- and Ru-doped SnO₂-Sb anodes with high stability in alkaline medium. ACS Applied Materials and Interfaces. (6):22778-22789. doi:10.1021/am506958k.



The final publication is available at

<http://pubs.acs.org/doi/abs/10.1021/am506958k>

Copyright American Chemical Society

Article

Pt- and Ru-doped SnO₂-Sb anodes with high stability in alkaline medium

Raúl Berenguer, Juan Manuel Sieben, Cesar Quijada, and Emilia Morallon

ACS Appl. Mater. Interfaces, **Just Accepted Manuscript** • DOI: 10.1021/am506958k • Publication Date (Web): 02 Dec 2014Downloaded from <http://pubs.acs.org> on December 3, 2014**Just Accepted**

“Just Accepted” manuscripts have been peer-reviewed and accepted for publication. They are posted online prior to technical editing, formatting for publication and author proofing. The American Chemical Society provides “Just Accepted” as a free service to the research community to expedite the dissemination of scientific material as soon as possible after acceptance. “Just Accepted” manuscripts appear in full in PDF format accompanied by an HTML abstract. “Just Accepted” manuscripts have been fully peer reviewed, but should not be considered the official version of record. They are accessible to all readers and citable by the Digital Object Identifier (DOI®). “Just Accepted” is an optional service offered to authors. Therefore, the “Just Accepted” Web site may not include all articles that will be published in the journal. After a manuscript is technically edited and formatted, it will be removed from the “Just Accepted” Web site and published as an ASAP article. Note that technical editing may introduce minor changes to the manuscript text and/or graphics which could affect content, and all legal disclaimers and ethical guidelines that apply to the journal pertain. ACS cannot be held responsible for errors or consequences arising from the use of information contained in these “Just Accepted” manuscripts.



1
2
3
4
5
6
7 Pt- and Ru-doped SnO₂-Sb anodes with high
8
9
10
11 stability in alkaline medium
12
13
14
15

16 *Raúl Berenguer^a, Juan Manuel Sieben^b, César Quijada^c, Emilia Morallón^{d,*}*
17

18
19 ^a Universidad de Málaga, Andalucía Tech, Departamento de Ingeniería Química, 29071 Málaga,
20 Spain.
21

22
23 ^b Instituto de Ingeniería Electroquímica y Corrosión and CONICET, Universidad Nacional del
24 Sur, Av. Alem 1253, (B8000CPB) Bahía Blanca, Argentina.
25

26
27 ^c Departamento de Ingeniería Textil y Papelera, Universidad Politécnica de Valencia, Plaza de
28 Ferrándiz y Carbonell, E-03801 Alcoy (Alicante), Spain.
29

30
31 ^d Departamento de Química Física e Instituto Universitario de Materiales, Universidad de
32 Alicante, Apartado 99, E-03080 Alicante, Spain.
33
34
35
36
37
38
39
40
41
42
43
44
45
46
47
48
49
50
51
52
53
54
55
56
57
58
59
60

Abstract

Different Pt- and Ru-doped Ti/SnO₂-Sb electrodes were synthesized by thermal decomposition. The effect of the gradual substitution of Sb by Ru in the nominal composition on the physicochemical and electrochemical properties were evaluated. The electrochemical stability of the electrodes was estimated from accelerated tests at 0.5 A g⁻¹ in 1M NaOH. Both as-synthesized and deactivated electrodes were thoroughly characterized by scanning electron microscopy (SEM), energy-dispersive X-ray microanalysis (EDX), transmission electron microscopy (TEM), X-Ray photoelectron spectroscopy (XPS) and X-Ray diffraction analysis (XRD). The incorporation of a small amount (about 3 at.%) of both Pt and Ru into the SnO₂-Sb electrodes produced a 400-times increase in their service life in alkaline medium, with no remarkable change in the electrocatalysis of the Oxygen Evolution Reaction (OER). It is concluded that the deactivation of the electrodes is promoted by alkaline dissolution of metal species and coating detachment at high potentials. The introduction of Pt has a coating compacting effect, and Ru(IV), at low amounts until 9.75 at.%, replaces the Sn(IV) cations in the rutile-like SnO₂ structure to form a solid solution that strongly increases the stability of the electrodes. The observed Ru segregation and decreased stability for larger Ru contents (x > 9.75 at. %), together with the selective dissolution of Ru after deactivation, suggest that the formation of a homogeneous (Ru_δSn_{1-δ})O₂ single-phase is crucial for the stabilization of these electrodes.

Keywords: DSA electrodes, doped tin dioxide electrodes, electrochemical stability, ruthenium oxide, alkaline solutions.

1. Introduction

Due to their unique properties and extremely high versatility, transition metal oxides (TMOs) have received a great interest as electrodes in many electrochemical applications.¹⁻¹⁷ Thus, they have been widely used in the chlor-alkali industry,² and multiple processes using electrolyzers,²⁻⁴ and constitute promising electrode materials for more sustainable and environmentally-friendly technologies in water remediation⁵⁻¹² and energy storage and conversion.¹³⁻¹⁶ Apart from a suitable performance, the economics and feasibility of the TMOs electrodes in these applications largely depend on their service life at operation conditions.^{1,17}

The tremendous success of some active TMOs (RuO_2 , IrO_2 , Co_3O_4 , etc.) supported onto a Ti substrate (the so-called dimensionally stable anodes, DSA), can be associated to their high stability and long lifetime at high potentials in aqueous electrolytes, where the oxygen evolution reaction (OER) occurs, as well as their good catalytic activity for this reaction, what provide lower cell-voltages and better faradic efficiencies in multiple processes.^{1,2,17} Nevertheless, for some applications, such as the electrochemical degradation of pollutants in wastewater,⁵⁻¹² the electrodes should have not only a good stability but also a high overpotential for the OER side-reaction.

The composition and the nature of the oxide coating strongly affect the stability and electrochemical activity of these DSA electrodes.^{1,17-19} Due to their high OER overpotential, considerably lower cost and innocuous character, the Sb-doped SnO_2 electrodes²⁰⁻²² have been found to be, among different choices, the most promising alternatives to the more expensive and fragile Boron-Doped Diamond (BDD) electrodes,^{12,23,24} and the more harmful, lead-leaching, PbO_2 -based electrodes.²⁵ Unfortunately, their anodic stability is remarkably low.^{20,21,26,27}

1
2
3 Although different approaches have been proposed to increase the stability of the SnO₂-based
4 electrodes, most of them focused on acid electrolytes,^{21,28,29,30} while the stability enhancement in
5 alkaline medium has received less attention.³¹ In general, the combination of SnO₂-based
6 electrodes with active species (Pt, Ir, Ru) enhances their stability, but it simultaneously increases
7 the catalytic activity towards the OER and the cost of the electrodes; however, the optimization
8 of the amount of active metal has not been often considered.⁵⁻¹² In addition, these investigations
9 mainly determined the service life of the electrodes without deepening into a detailed
10 characterization of fresh and deactivated electrodes. So the understanding of the stabilization
11 effect and the deactivation mechanisms need further research.
12
13
14
15
16
17
18
19
20
21
22
23

24
25
26 Considering the growing application of electrochemistry in different fields, the development of
27 high-performance electrodes for alkaline electrolytes gathering both high OER-overpotential and
28 stability, is very interesting for multiple electrochemical applications, such as fuel cells, electro-
29 oxidation of compounds in electrosynthesis or the electrochemical degradation of pollutants,
30 etc.¹⁻¹⁷ For this purpose, the establishment of structure-composition vs. stability correlations and
31 the investigation of the deactivation mechanism of the electrodes are of utmost importance to
32 further propose new stabilization strategies.
33
34
35
36
37
38
39
40
41
42

43 It has been previously found that the introduction of a small amount (3 at. %) of Pt enhances the
44 service life of Sb-doped SnO₂ electrodes in acidic electrolyte by two orders of magnitude,²⁸ also
45 showing an even higher efficiency for phenol electro-oxidation in the same medium; however,
46 higher amounts of Pt (13 at. %) decrease their performance.³² On the other hand, it is well
47 documented that RuO₂ exhibits a high catalytic activity and stability for the OER.^{31,33} The
48 stability of binary (Sn-Ru)O₂ oxides were previously studied, but experiments were restricted to
49 acidic medium^{29,34} and the influence of Sb or Pt was not considered. Consequently, in this work
50
51
52
53
54
55
56
57
58
59
60

1
2
3 we have investigated the influence of Pt, as well as the progressive substitution of Sb by Ru in
4
5 the nominal composition of SnO₂-Sb/Ti electrodes, on the physicochemical properties and the
6
7 electrochemical response of the electrode. For this purpose, different SnO₂-Sb(13-x)-Pt(3)-
8
9 Ru(x)/Ti electrodes ($0 \leq x$ (at. %) ≤ 13), were synthesized by thermal decomposition and
10
11 thoroughly characterized, before and after deactivation. The electrochemical stability of the
12
13 electrodes was estimated by accelerated tests at 0.5 A g⁻¹ in 1 M NaOH. The structural properties
14
15 were studied by SEM, TEM and XRD, whereas the chemical composition was followed by EDX
16
17 and XPS. The electrochemical behavior as well as the catalytic activity towards the OER was
18
19 analyzed by cyclic voltammetry and Tafel measurements, respectively, in the same electrolyte.
20
21 Furthermore, SnO₂-Sb/Ti, SnO₂-Ru/Ti and RuO₂/Ti electrodes were prepared and characterized
22
23 by the same techniques.
24
25
26
27
28
29

30 2. Experimental

31
32
33 Four types of tetragonal rutile-like oxide electrodes (with composition in brackets expressed as
34
35 metal atomic percentage), SnO₂-Sb(13 at. %), SnO₂-Sb(13-x)-Pt(3)-Ru(x) (with $0 \leq x \leq 13$ at.
36
37 %), SnO₂-Ru(13 at. %) and RuO₂, were synthesized by the thermal decomposition method
38
39 following the procedure described elsewhere.³³ Briefly, the precursor solutions, consisting of
40
41 SnCl₄ · 5H₂O, SbCl₃, H₂PtCl₆ · 6H₂O and RuCl₃ · nH₂O in absolute ethanol and HCl with the
42
43 desired nominal composition, were spread over pre-treated Ti plates (1 cm × 1 cm × 0.05 cm;
44
45 Goodfellow 99.6 %) by brushing. Previously, the Ti plates were degreased in acetone, etched in a
46
47 boiling 10 % oxalic acid solution for 1 h and finally rinsed with distilled water. The sample was
48
49 dried at 70 °C in order to evaporate the solvent and the metal oxides were formed by calcination
50
51 at 400 °C for 10 min. This procedure was successively repeated to increase the oxide loading up
52
53
54
55
56
57
58
59
60

to ca. 1.5–2.0 mg cm⁻². The number of deposition steps for these loadings were between 20 and 25. A final annealing step was carried out for 60 min at 600 °C.

The nominal composition of the precursor solution is presented in Table 1. In all cases, the total metal cation concentration was kept constant at 0.5 m.

Table 1. Nominal composition of the precursor solutions for the different electrodes.

Electrode	(x) ^a	(g) salt precursor/100 (g) solution				Ethanol (ml)
		SnCl ₄ · 5H ₂ O	SbCl ₃	H ₂ PtCl ₆ · 6H ₂ O	RuCl ₃ · nH ₂ O	
SnO ₂ -Sb/Ti	0.00	10.000	1.000	---	---	112.7
SnO ₂ -Sb(13-x)- Ru(x)-Pt/Ti	0.00	10.000	1.000	0.400	---	112.4
	3.25	10.000	0.750	0.400	0.287	112.4
	6.50	10.000	0.500	0.400	0.573	112.3
	9.75	10.000	0.250	0.400	0.860	112.3
	13.00	10.000	---	0.400	1.146	112.2
SnO ₂ -Ru/Ti	13.00	10.000	---	---	1.146	112.5
Ti/RuO ₂ /Ti	100	---	---	---	5.186	50.0

^a(x): nominal Ru percentage

2.2 Physicochemical characterization

The surface morphology of the electrodes was studied by scanning electron microscopy (SEM) in a Hitachi S-3000N electron microscope coupled to a Rontec X-ray detector for energy dispersive X-ray (EDX) microanalysis. The microstructure and crystallinity were characterized by X-ray diffraction (XRD) in a KRISTALLOFLEX K 760-80F diffractometer (Bruker D8-

1
2
3 Advance) by using a Ni-filtered Cu K α radiation ($\lambda = 1.5416 \text{ \AA}$). Diffraction data points were
4 recorded stepwise within $2\theta = 20\text{-}80^\circ$ at a scan rate of $0.03^\circ \text{ min}^{-1}$ with a scan step of 0.05° in
5
6
7
8
9
10
11
12
13
14
15
16
17
18
19
20
21
22
23
24
25
26
27
28
29
30
31
32
33
34
35
36
37
38
39
40
41
42
43
44
45
46
47
48
49
50
51
52
53
54
55
56
57
58
59
60

Advance) by using a Ni-filtered Cu K α radiation ($\lambda = 1.5416 \text{ \AA}$). Diffraction data points were recorded stepwise within $2\theta = 20\text{-}80^\circ$ at a scan rate of $0.03^\circ \text{ min}^{-1}$ with a scan step of 0.05° in 2θ . Cell parameters were calculated by a computer program using the peak position obtained after fitting the experimental range with a pseudo-Voigt function per peak plus a background line. Line-broadening analysis was performed to determine the average crystallite size.

The morphology and particle size were analyzed by transmission electron microscope (TEM) in a JEOL equipment (JEM-2010) with an accelerating voltage of 200 keV. X-ray photoelectron spectroscopy (XPS) measurements were carried out by a VG-Microtech Multilab 3000 spectrometer with Mg K α radiation ($h\nu = 1256.3 \text{ eV}$) at base pressure of 5×10^{-10} mbar in the analysis chamber. Binding energies were referenced against the main C(1s) line of adventitious carbon impurities at 284.6 eV. Peak energies were given to an accuracy of 0.2 eV and peak areas were normalized by using appropriate atomic sensitivity factors.

2.3 Electrochemical measurements

The electrochemical measurements were performed on an Autolab PGSTAT 30 potentiostat controlled by GPES EcoChimie software using a conventional three-electrode glass cell. The counter electrode was a spiral of platinum wire of 12 cm length and 0.5 mm of diameter and the potentials are referred to a reversible hydrogen electrode (RHE) immersed in the same solution. The aqueous 0.1 M NaOH solutions were de-oxygenated by N₂ bubbling. All solutions were prepared with purified water obtained from an Elga Labwater Purelab system (18.2 M Ω cm). In these studies, cyclic voltammetry (CV) measurements were performed between different potential limits at a scan rate between 1 and 500 mV s⁻¹. The current densities were calculated using the apparent geometric area of the electrodes (2 cm²). The voltammetric charges (q*)

1
2
3 corresponding to electrochemically active surface areas were determined by integrating the area
4 of the cyclic voltammograms. The electrocatalytic activity towards OER was investigated in
5 aqueous 0.1 M NaOH solution by galvanostatic experiments at current densities lower than 5 mA
6 cm^{-2} at a scan rate of 3 $\mu\text{A s}^{-1}$.
7
8
9

10
11
12 The accelerated service-life tests were performed by anodic polarization of the different
13 electrodes at 0.5 A cm^{-2} in a 1 M NaOH solution at a controlled temperature of 25 °C. The anode
14 potential was measured as a function of time, and the electrode was considered to be deactivated
15 when the potential increased to 5 V above its initial value. In these experiments a Ag/AgCl/Cl⁻
16 (sat.) electrode served as the reference electrode. The electrolyte composition after the anodic
17 deactivation treatment was determined by ICP-OES analysis (Perkin Elmer 7300 DV).
18
19
20
21
22
23
24
25
26
27

28 29 **3. Results and discussion**

30 31 32 3.1. Physicochemical characterization.

33 34 35 3.1.1. Surface morphology.

36
37
38 The as-prepared SnO₂-Sb/Ti, RuO₂/Ti and SnO₂-Sb-Pt/Ti electrodes (Fig. 1a,c,e, respectively)
39 exhibit the typical cracked-mud morphology of these metal oxide coatings prepared by thermal
40 decomposition.^{20,21,28,35} These surface cracks may be produced during the electrode cooling to
41 room temperature^{20,28} and/or by solvent evaporation during heating stages.³⁶ Nevertheless, the
42 incorporation of a small amount of Pt (3 at. %) in the SnO₂-Sb layer (Fig. 1e) significantly
43 reduces the number of cracks and pores, producing a compacting effect that has been attributed
44 to a strengthening and shortening of the oxide intercolumn bondings caused by Pt aggregates on
45 the surface of SnO₂ grains.³⁷
46
47
48
49
50
51
52
53
54
55
56
57
58
59
60

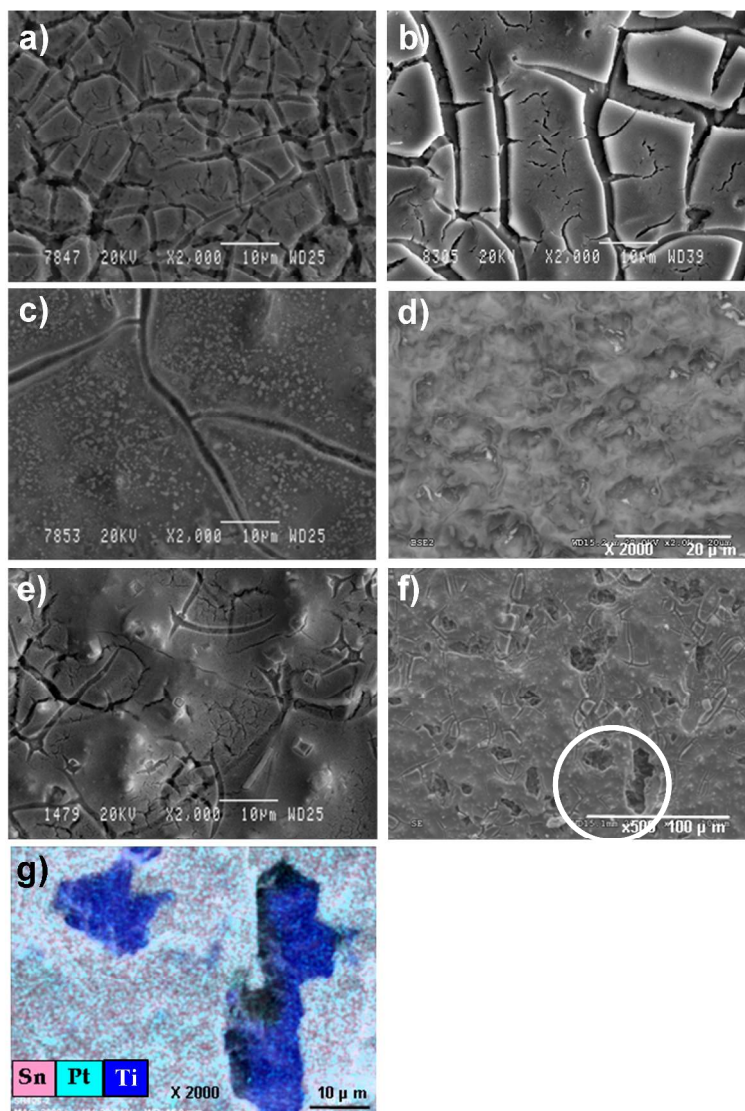


Figure 1. SEM images of (a) fresh SnO₂-Sb/Ti electrode, (b) deactivated SnO₂-Sb/Ti electrode, (c) fresh RuO₂/Ti electrode, (d) deactivated RuO₂/Ti electrode, (e) fresh SnO₂-Sb-Pt/Ti electrode, (f) deactivated SnO₂-Sb-Pt/Ti electrode and (g) EDX-mapping of the circled area in (f)

The surface cracks on the SnO₂-Sb-Pt/Ti oxide layer disappear and porosity dramatically increases upon substituting Sb with 3.25 at. % Ru in the nominal composition (Fig. 2a). However, further incorporation of Ru (6.50-9.75 at. %) gradually reduces the oxide surface

roughness (Fig. 2b-c) until the cracked-mud structure is restored again at a ruthenium content of 13 at. % (Fig. 2d).³³ In addition, the presence of small grains is also observed in these latter electrodes (Fig. 2d). The EDX mapping shows that the small grains contain a high concentration of Ru, indicating phase separation. The phase separation/segregation of Ru in Sn-Ru mixed oxides synthesized by traditional methods has been reported in the literature.³⁸⁻⁴⁰

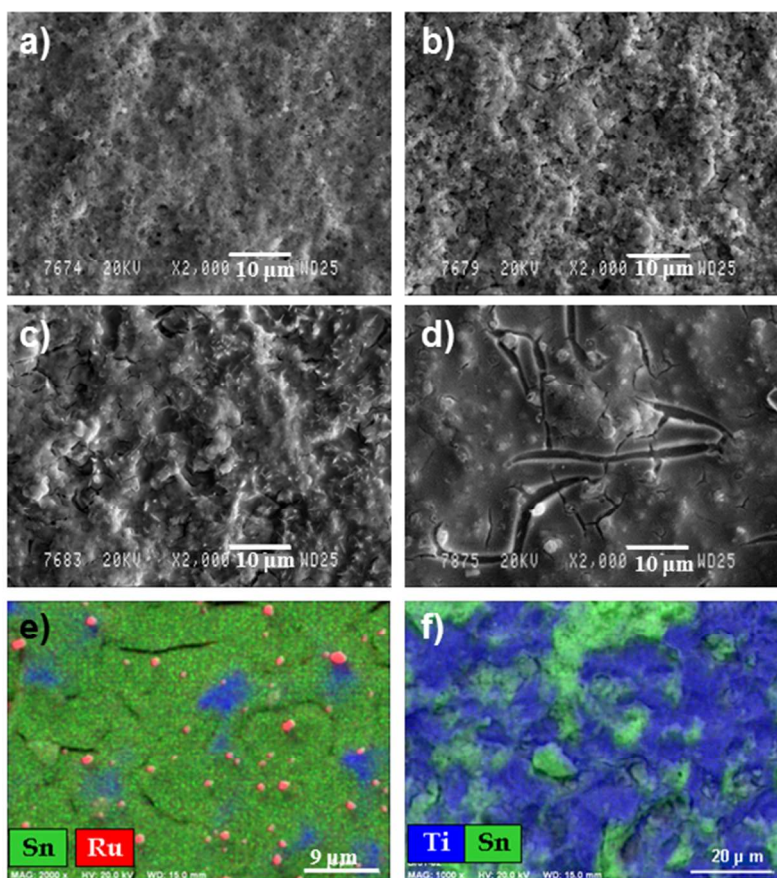


Figure 2. SEM images of fresh $\text{SnO}_2\text{-Sb}(13\text{-}x)\text{-Pt-Ru}(x)/\text{Ti}$ electrodes with $x = 3.25$ at. % (Ru) (a), $x = 6.50$ at. % (Ru) (b), $x = 9.75$ at. % (Ru) (c), $x = 13.00$ at. % (Ru) (d), fresh $\text{SnO}_2\text{-Ru/Ti}$ electrode (e); and deactivated $\text{SnO}_2\text{-Sb}(13\text{-}x)\text{-Pt-Ru}(x)/\text{Ti}$ electrode; $x = 3.25$ at.% Ru (f).

3.1.2. Chemical composition.

1
2
3 EDX spectra and mappings registered at different regions of the electrode surfaces showed a
4
5 homogeneous distribution of the elements in the oxide films. The low signals from the
6
7 underlying Ti evidenced that a good coverage of the substrate was achieved. According to the
8
9 methodology reported elsewhere,^{28,33} the coating thickness estimated from oxide loadings ranged
10
11 between 2 and 3 μm . The nominal and experimental compositions of the different mixed metal
12
13 oxides were expressed as the amount of individual metals with respect to the total metal content,
14
15 M, (atomic ratios) (Table 2). Comparisons between bulk and surface compositions, obtained by
16
17 EDX and XPS analysis, respectively, provided some insight into the distribution of the different
18
19 species. The fairly good correlation between the nominal and EDX experimental Sn/M and Sb/M
20
21 ratios in SnO₂-Sb/Ti and SnO₂-Sb-Pt/Ti (x = 0.00 %) electrodes points out that Sn and Sb were
22
23 successfully combined in the desired proportions, although Sb depletion occurs at the surface of
24
25 these electrodes.
26
27
28
29
30
31
32
33
34
35
36
37
38
39
40
41
42
43
44
45
46
47
48
49
50
51
52
53
54
55
56
57
58
59
60

Table 2. Nominal and experimental EDX and XPS atomic ratios with respect to the total metal content (M) obtained for (fresh) and deactivated (deact.) electrodes.

Electrode (x)	Sn/M ^a				Sb/M				Pt/M				Ru/M				I _{OH} /I _{OM} ^b		
	Nom.	EDX fresh	XPS fresh	XPS deact	Nom.	EDX fresh	XPS fresh	XPS deact	Nom.	EDX fresh	XPS fresh	XPS deact	Nom.	EDX fresh	XPS fresh	XPS deact	XPS fresh	XPS deact	
SnO ₂ -Sb/Ti	-	0.87	0.88	0.94	0.92	0.13	0.12	0.06	0.07	-	-	-	-	-	-	-	-	0.27	0.12
	0.00	0.84	0.83	0.88	0.90	0.13	0.11	0.07	0.05	0.03	0.06	0.04	0.06	-	-	-	-	0.24	0.18
SnO ₂ -	3.25	0.84	0.69	0.66	0.73	0.10	0.24	0.32	0.10	0.03	0.04	0.02	0.17	0.03	0.03	0.00	0.00	0.54	0.34
Sb(13-x)-	6.50	0.84	0.69	0.71	0.79	0.06	0.19	0.21	0.07	0.03	0.05	0.06	0.14	0.06	0.07	0.02	0.00	0.32	0.27
Pt-Ru(x)/Ti	9.75	0.84	0.72	0.90	0.85	0.03	0.10	0.05	0.09	0.03	0.06	0.03	0.06	0.10	0.12	0.02	0.00	0.23	0.12
	13.00	0.84	0.78	0.96	0.87	-	-	-	-	0.03	0.06	0.02	0.11	0.13	0.16	0.02	0.02	0.27	0.30
SnO ₂ -Ru/Ti	-	0.87	0.79	0.96	0.98	-	-	-	-	-	-	-	-	0.13	0.21	0.04	0.02	0.55	0.26
RuO ₂ /Ti	-	-	-	-	-	-	-	-	-	-	-	-	-	1.00	1.00	1.00	1.00	0.00	0.74

a Total metal content, M = Sn + Sb + Pt + Ru

b Adsorbed oxygen O-H (OAds.) to oxide-lattice oxygen M-O (Ooxid.) photoemission intensities ratio (corrected values from deconvoluted O(1s), C(1s) and Ti(2p-XPS spectra): IOH = [OAds.] - [C-OH] and IOM = [Ooxid.] - 2[Ti].

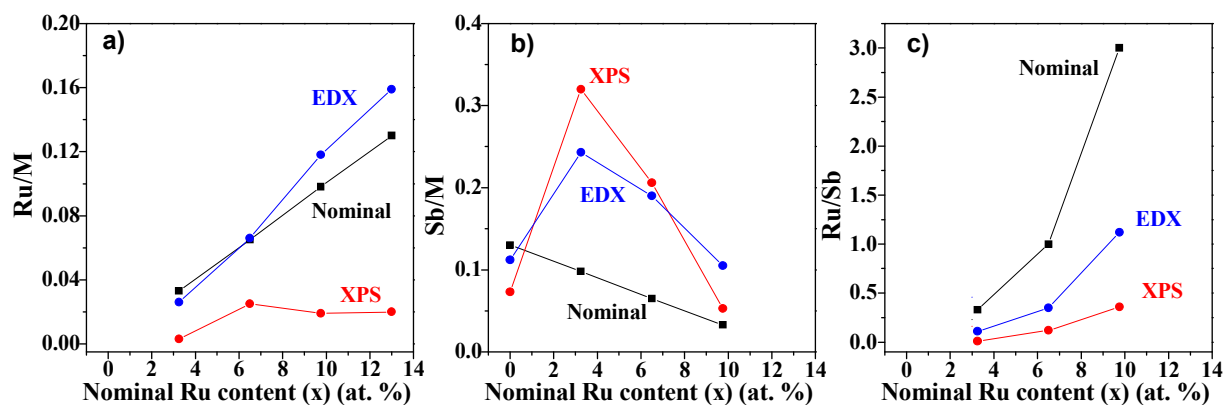


Figure 3. EDX and XPS atomic ratios relative to the total metal content (M) of SnO₂-Sb(13-x)-Pt-Ru(x)/Ti electrodes as a function of the nominal Ru content: a) Ru/M; b) Sb/M and c) Ru/Sb.

1
2
3 In the same manner, the similarity between nominal and EDX-obtained Ru/M ratios shows that
4 the amount of Ru introduced in the SnO₂-Sb(13-x)-Pt-Ru(x)/Ti electrodes approaches quite well
5 the desired one, whereas the surface Ru content (XPS ratio) remains almost constant and much
6 lower than the nominal one (Fig. 3a). As shown in Fig. 3b and Table 1, the introduction of a low
7 Ru content (x = 3.25 at. %) produces a marked enrichment in Sb and a marked depletion in Sn, in
8 both the bulk and the surface of the electrodes. A further increment in the Ru content gradually
9 increases the Sn/M ratio and reduces the Sb/M ratio to values (for x = 9.75 at. %) closer to those
10 obtained in the absence of Ru (x = 0.00 at. %) (Table 1). On the other hand, the comparison
11 among the nominal and EDX and XPS experimental Ru/Sb ratios (Fig. 3c.) shows that only
12 about one third of Sb is replaced by Ru. This may indicate that Ru does not effectively replace
13 Sb in the mixed oxide, but it may replace Sn in the rutile-like lattice, hence explaining its
14 depletion. Finally, the amount of Pt (bulk) introduced in the coatings is above (almost double)
15 the nominal one, regardless of the Ru content (Table 1), while the Pt surface content varies above
16 and below the nominal one with no clear trend. However, a clear surface depletion of Ru with
17 respect to both its nominal and experimental bulk values is observed in the whole set of SnO₂-
18 Sb(13-x)-Pt(3)-Ru(x)/Ti electrodes.

3.1.3. Surface chemical state.

19
20
21
22
23
24
25
26
27
28
29
30
31
32
33
34
35
36
37
38
39
40
41
42
43
44
45
46 The Sn(3d) spectra of the different SnO₂-based electrodes (Fig. 4a) show two peaks at 487.0 eV
47 and 495.4 eV, typically assigned to the Sn 3d_{3/2} and 3d_{5/2} states from the spin-orbital
48 splitting,^{41,42} which may correspond to either SnO, SnO₂ or Sn(OH)_x species.^{41,42} Since the XPS
49 spectrum (not shown) does not exhibit any Sn(5s) peak attributed to SnO, the Sn(3d) signals are
50 assigned to SnO₂.⁴¹ In agreement with data previously reported,⁴³ the incorporation of low Pt
51 doping levels in mixed Sn-Sb oxides (Fig. 4a, x = 0.00 %) does not produce any change neither in
52
53
54
55
56
57
58
59
60

the Sn(3d) core-level binding energy nor in their energy width and symmetry with respect to undoped materials. This result suggests that the electronic structure of the SnO₂ lattice is unaffected by Pt atoms at such a low content.⁴¹ The Pt 4f_{7/2} core level photoemission peak observed for the SnO₂-Sb(13-x)-Pt-Ru(x)/Ti electrodes can be separated into three main contributions and three satellite peaks (Fig. 4c). These peaks are associated with the presence of metallic platinum (Pt(0)) and Pt(II) and Pt(IV) species), and their relative concentration was found to vary randomly among the different electrodes.⁴³

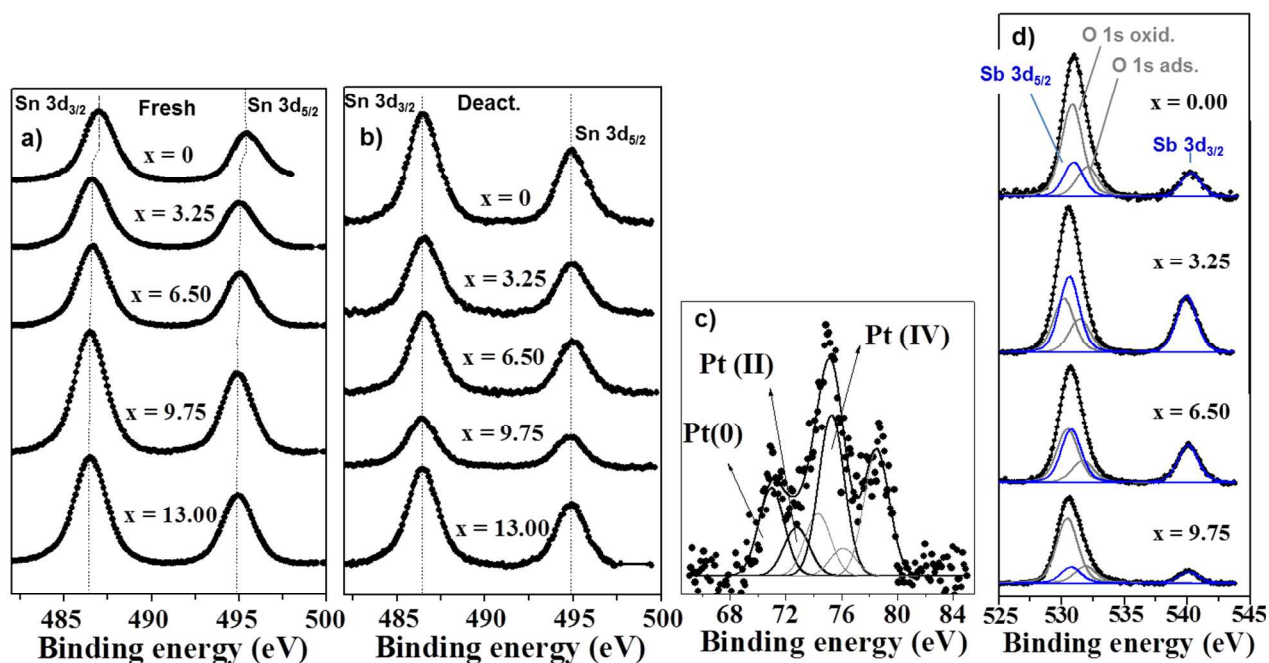


Figure 4. Sn(3d) XPS spectra of (a) fresh SnO₂-Sb(13-x)-Pt-Ru(x)/Ti electrodes, (b) deactivated SnO₂-Sb(13-x)-Pt-Ru(x)/Ti electrodes; (c) Pt(4f) XPS spectrum of a fresh SnO₂-Sb-Pt/Ti electrode; and (d) Sb(3d) XPS spectra of fresh SnO₂-Sb(13-x)-Pt-Ru(x)/Ti electrodes.

1
2
3 On the other hand, the XPS spectra in the energy region between 525 eV and 544 eV revealed
4 the presence of another two peaks (Fig. 4d). The peak at 540 eV corresponds to the Sb 3d_{3/2}
5 signal, while that at 531 eV is composed of the O(1s) (at 531 eV) together with the Sb 3d_{5/2}
6 signals. The deconvolution of the Sb 3d_{3/2} signal revealed that the largest fraction of Sb in the
7 SnO₂-Sb/Ti electrode has a 5+ oxidation state (contribution at 530.6 eV^{28,43-46}), although Sb(III)
8 (22 at. %) was also observed in this electrode.^{41,46} Some authors have indicated that Sb(III) is
9 preferentially located on the surface and grain boundaries of the SnO₂-Sb film.^{41,46} On the
10 contrary, the Sb 3d_{3/2} peak in SnO₂-Sb(13-x)-Pt-Ru(x)/Ti electrodes (Fig. 4d) can be
11 satisfactorily fitted with a single photoemission contribution corresponding to Sb atoms in a 5+
12 charge state (usually represented as SnO₂-Sb₂O₅). This is in agreement with the results of
13 Montilla et al.,⁴³ who found that the presence of a small Pt content on the electrode surface
14 promotes the complete oxidation of Sb in the oxide coating. With the theoretical peak intensity
15 ratio and splitting of the Sb(3d) spin-orbit doublet (1.44 and 10.7 eV, respectively), we used the
16 Sb 3d_{3/2} peak to correct the O(1s) photoemission line from the Sb 3d_{5/2} interference.^{43,45} After the
17 correction, the O(1s) signal could be deconvoluted into two peaks (Fig. 4d). The major peak at
18 530.9 eV is associated with oxygen directly bonded to a metal atom (metal oxides) and the minor
19 one (532.1 eV) is related to oxygen bonded to metal hydroxides or hydrated species on the
20 surface.^{41,43}
21
22
23
24
25
26
27
28
29
30
31
32
33
34
35
36
37
38
39
40
41
42
43
44
45
46
47
48
49
50
51
52
53
54
55
56
57
58
59
60

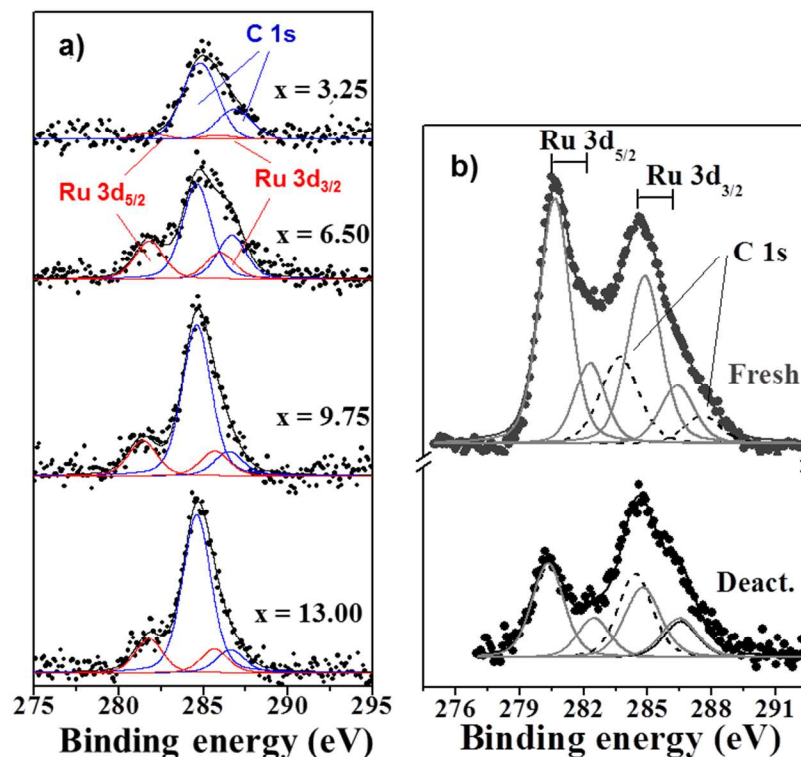


Figure 5. Ru(3d) XPS spectra of (a) fresh $\text{SnO}_2\text{-Sb}(13-x)\text{-Pt-Ru}(x)/\text{Ti}$ electrodes and (b) fresh and deactivated RuO_2/Ti electrodes.

The introduction of Ru ($\text{SnO}_2\text{-Sb}(13-x)\text{-Pt-Ru}(x)/\text{Ti}$ electrodes) leads to the appearance of Ru $3d_{5/2}$ and $3d_{3/2}$ peaks at 282.3 eV and 284.8 eV, respectively, which overlap with the region of C(1s) core level spectra of adventitious carbon (Fig. 5a). These two peaks are observed also in the spectrum of pure RuO_2/Ti electrode (Fig. 5b) and are assigned to ruthenium (IV) oxide.⁴⁷ Moreover, the progressive substitution of Sb by Ru in the nominal composition causes a band shift of Sn $3d_{5/2}$ and $3d_{3/2}$ peaks towards lower binding energies (Fig. 4a), whereas it does not cause a significant effect on the binding energy of Sb $3d_{3/2}$ and O(1s) (Fig. 4d). These results may indicate that there is no interaction between Sb and Ru species, but instead, a strong chemical interaction between Sn(IV) and Ru(IV) cations occurs.

3.1.4. Structural characterization.

1
2
3 Fig. 6a shows the XRD diffraction patterns of the as-prepared $\text{SnO}_2\text{-Sb}(13\text{-}x)\text{-Pt-Ru}(x)/\text{Ti}$
4 electrodes. For comparison purposes, the XRD diffraction peaks of RuO_2 and the Ti substrate are
5 also included in this figure. The XRD diffractogram of the $\text{SnO}_2\text{-Sb-Pt/Ti}$ electrode is very
6 similar to that of $\text{SnO}_2\text{-Sb/Ti}$ (Fig. S2) with sharp peaks corresponding to the tetragonal rutile-
7 like structure of SnO_2 cassiterite.⁴⁴ In a similar way, the observed XRD of the RuO_2/Ti electrode
8 (Fig. 6a) is also in agreement with the tetragonal rutile-like structure of RuO_2 (Table 2). The
9 replacement of Sb by Ru in the nominal composition does not result in the appearance of new
10 diffraction peaks. However, the progressive incorporation of Ru into the oxide coating shifts the
11 SnO_2 diffraction peaks to higher Bragg angles, although this increase is small above $x = 9.75$ at.
12 % (Fig 6b). As it is shown in Table 2, the increase in Bragg angles involves a gradual reduction
13 in the unit-cell parameters and, consequently, in the volume of the unit-cell. This indicates that
14 Ru(IV), which has a smaller ionic radius than Sn(IV) (0.76 Å against 0.83 Å), is incorporated
15 into the cationic SnO_2 sublattice to form a solid solution $(\text{Ru}_\delta\text{Sn}_{1-\delta})\text{O}_2$, leading to the contraction
16 of the rutile-like lattice.^{39,47,48} The formation of such a solid solution is strongly supported by the
17 marked effect of Ru in the Sn(3d) binding energies (Fig. 4a). Nevertheless, the diffraction peaks
18 for $x = 9.75$ at. % start to display certain asymmetry that becomes more important at the highest
19 Ru content. This asymmetry is more noticeable in the $\text{SnO}_2\text{-Ru/Ti}$ electrode prepared in the same
20 conditions (Fig. 6c). The deconvolution of these diffraction peaks reveals that the asymmetry
21 corresponds to the formation of a RuO_2 phase. Both the appearance of peak asymmetry and the
22 leveling off in the Bragg angle shift from $x = 9.75$ at. % suggest that the mixed oxide reaches the
23 solubility limit of Ru cations into the rutile-like SnO_2 lattice, so Ru starts to segregate as RuO_2
24 phase.
25
26
27
28
29
30
31
32
33
34
35
36
37
38
39
40
41
42
43
44
45
46
47
48
49
50
51
52
53
54
55
56
57
58
59
60

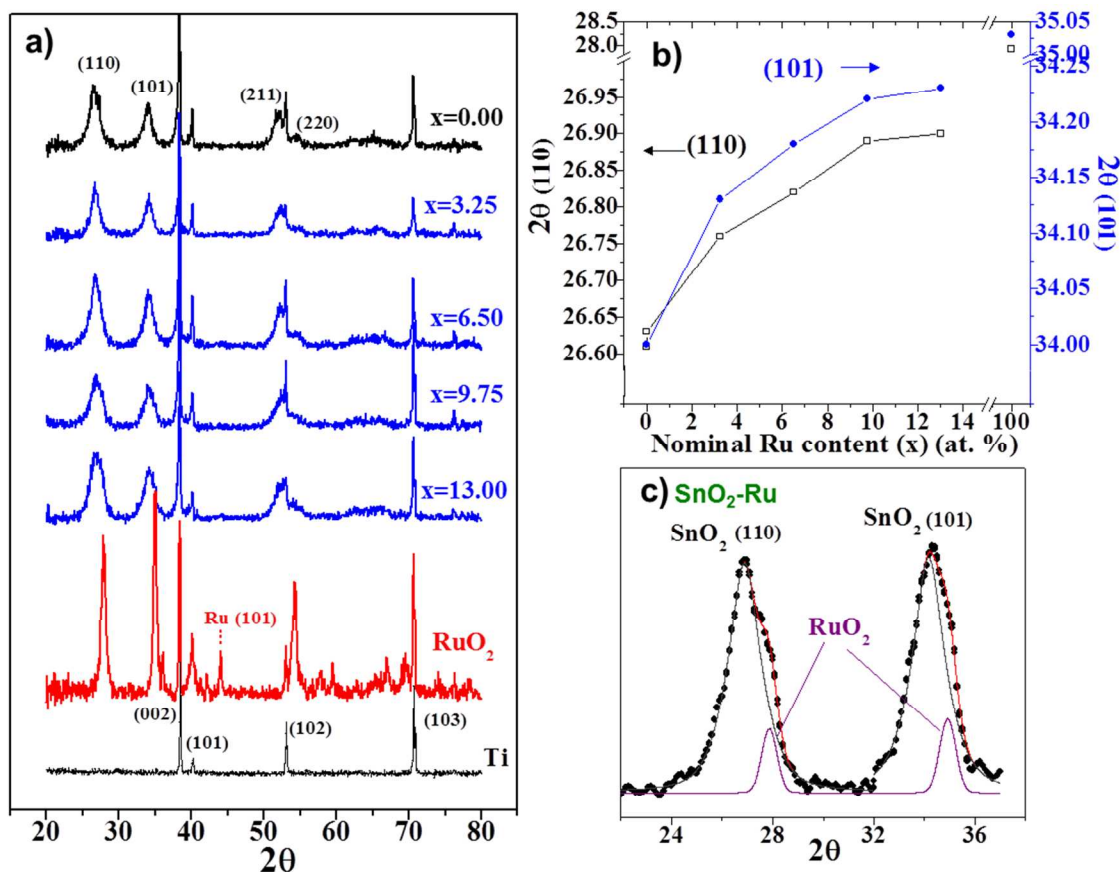


Figure 6. (a) X-ray diffraction patterns of fresh SnO₂-Sb(13-x)-Pt-Ru(x)/Ti electrodes and RuO₂/Ti electrode; (b) (110) and (101) peak position as a function of the nominal Ru content; (c) deconvolution of (110) and (101) peaks for SnO₂-Ru/Ti electrode.

In spite of the structural changes, Table 3 shows that the addition of the doping metals like Ru, Sb or Pt, produces almost no effect in the average crystallite size of the different oxides, which ranges between 5.2-5.8 nm. This crystallite size is in agreement with the average particle size (around 5-10 nm), observed by TEM (Fig. 7). The figure includes TEM images of SnO₂-Sb(13-x)-Pt-Ru(x) oxides with different Ru contents. The oxides consist of highly aggregated particles with ellipsoidal-like morphology, in agreement with other transition metal oxides prepared by thermal decomposition.⁴⁹ In particular, specific phases characteristic of Sb, Pt, and Ru dopants

were not distinguished, in accordance with XRD results, and the lack of significant differences among the three images reveals that the introduction of Ru in the mixed solid solution ($\text{Ru}_\delta\text{Sn}_{1-\delta}\text{O}_2$) causes practically no effect in the microstructure of the oxides.

Table 3. Lattice parameters ($a = b$ and c) of the rutile-like structure, unit cell volume (V) and crystallite size (d_c) for the as-prepared electrodes calculated from XRD patterns.

Electrode	(x)	a (\AA) ^b	c (\AA) ^b	V (\AA^3) ^b	d_c ^c (nm)
SnO_2 , cassiterite ^a	-	4.740	3.190	71.7	-
SnO_2 -Sb/Ti	-	4.734	3.173	71.1	5.6
	0.00	4.730	3.173	71.0	5.7
	3.25	4.708	3.161	70.1	5.8
	6.50	4.697	3.154	69.6	5.5
	9.75	4.687	3.152	69.2	5.2
	13.00	4.685	3.147	69.1	5.2
SnO_2 -Ru/Ti	-	4.685	3.148	69.1	5.5
RuO_2 /Ti	-	4.504	3.113	63.1	13.2
RuO_2 ^a	-	4.499	3.107	62.9	-

^a JCPDS-International Centre for Diffraction Data.

^b Lattice parameters were calculated with the Bragg's equation.

^c Average crystallite size determined from (110), (101), (211) and (220) SnO_2 -phase reflections and Scherrer's equation. The width of the deconvoluted SnO_2 phase reflection was considered where segregation of RuO_2 occurs.

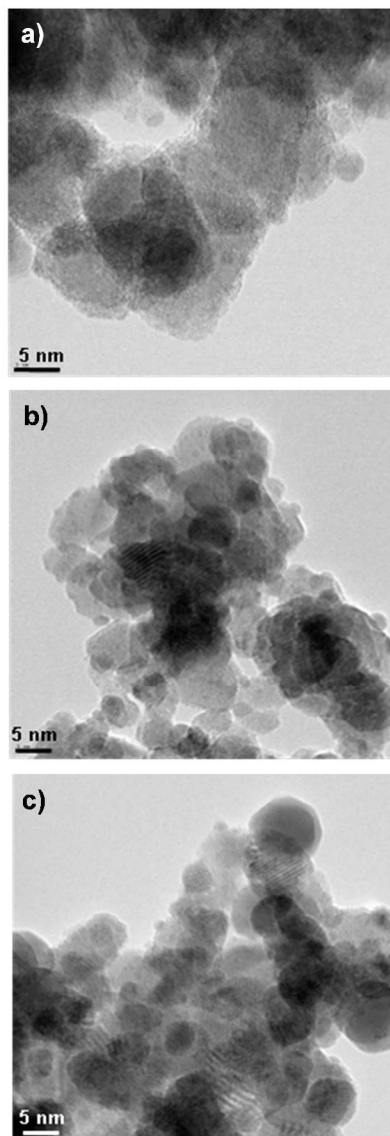


Figure 7. TEM images of fresh $\text{SnO}_2\text{-Sb}(13-x)\text{-Pt-Ru}(x)/\text{Ti}$ electrodes: (a) $x = 0.00$ at. % Ru; (b) $x = 6.50$ at. % Ru; (c) $x = 9.75$ at. % Ru.

3.2 Electrochemical measurements

3.2.1 Electrochemical behavior.

Fig. 8 shows the voltammetric response of the as-synthesized electrodes in alkaline medium. The voltammogram of $\text{SnO}_2\text{-Sb}/\text{Ti}$ electrode (Fig. 8a) shows no oxidation/reduction peaks and a

sharp current rise, corresponding to the oxygen evolution reaction (OER), at potentials above 1.8 V. These features are common to non-active oxides. In the presence of Pt ($x = 0.00$ at. %) (Fig. 8b), the onset of the OER is shifted to lower potentials (around 1.7 V) and the voltammogram includes a broad oxidation peak (between 0.7 and 1.4 V) and a much better-defined reduction counterpart (at ca. 0.65 V) attributed to the formation and reduction of surface platinum oxides (Pt/PtO_x) (A₁/C₁).²⁸

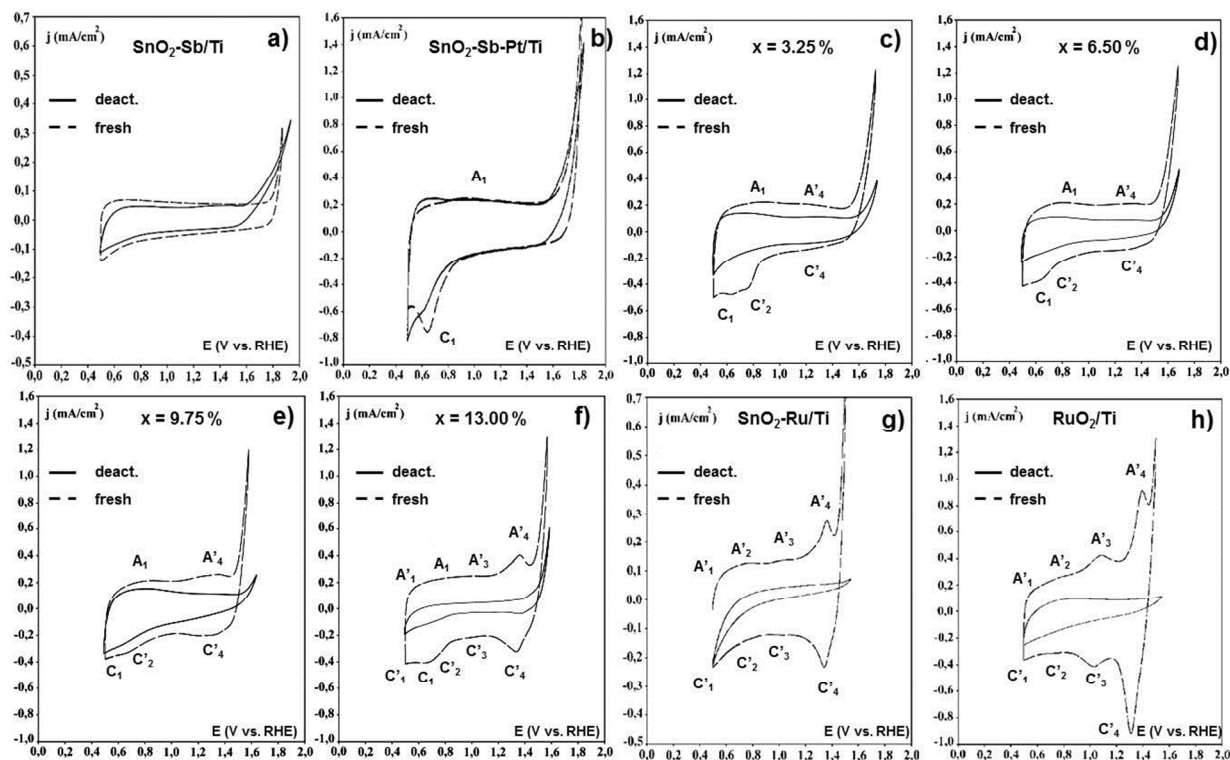


Figure 8. Steady cyclic voltammograms of fresh and deactivated electrodes in a 0.1M NaOH solution, (a) SnO₂-Sb/Ti electrode, SnO₂-Sb(13-x)-Pt-Ru(x)/Ti electrodes with (b) $x = 0.00$ at. %, (c) $x = 3.25$ at. %, (d) $x = 6.50$ at. %, (e) $x = 9.75$ at. %, (f) $x = 13.00$ at. %, (g) SnO₂-Ru/Ti electrode and (h) RuO₂/Ti electrode; $\nu = 20 \text{ mV s}^{-1}$.

The gradual introduction of Ru in SnO₂-based electrodes (Fig. 8 c-h,g) results in the appearance of various redox couples associated with the surface transitions of Ru in RuO₂ electrodes (Fig. 8h): i) Ru(II) ↔ Ru(III) (A₁'/C₁'), ii) Ru(III) ↔ Ru(IV) (A₂'/C₂'), iii) Ru(IV) ↔ Ru(VI) (A₃'/C₃') and iv) Ru(VI) ↔ Ru(VII) (A₄'/C₄').^{47,50} The current of these peaks increases with the Ru content. Furthermore, the onset potential of OER is shifted by about 0.1 V to less positive potentials than the observed for SnO₂-Sb-Pt/Ti electrode due to the electrocatalytic effect of Ru on the OER.

Table 3. Service life (SL) and service life efficiency (SLE), specific capacitance, roughness factor (Rf) and electrochemical porosity (P_e) for the as-prepared electrodes in 0.1M NaOH solution.

Electrode	(x)	SL (h)	SLE (A h mg ⁻¹)	Specific Capacitance (mF cm ⁻²)					Rf	P _e (Nom.)
				0.55 V	0.75 V	0.95 V	1.15 V	1.35 V		
SnO ₂ -Sb/Ti	-	0.6	0.2	3.1	2.6	2.4	2.1	2.0	389	0.09
	0.00	72	22	3.7	3.4	3.0	2.7	2.5	464	0.34
SnO ₂ -Sb(13-x)-Pt-Ru(x)/Ti	3.25	189	63	7.4	7.3	6.7	6.1	5.9	931	0.33
	6.50	210	75	7.2	7.2	6.7	6.3	6.3	900	0.32
	9.75	212	106	6.9	7.0	6.7	6.6	7.1	863	0.29
	13.00	86	25	6.1	6.1	5.4	5.9	8.5	761	0.21
SnO ₂ -Ru/Ti	-	116	35	3.4	3.5	3.5	3.6	8.6	450	0.10
RuO ₂ /Ti	-	640	181	6.8	7.5	8.5	12.1	20.7	85	0.19

Service life (SL) and service life efficiency (SLE, total charge passed per unit mass of deposited oxide) at 0.5 A cm⁻² in 1 M NaOH solution. The rest of parameters were obtained from voltammetric measurements in 0.1 M NaOH.

The capacitance of the electrodes in 0.1 M NaOH was measured at different potentials (Table 3) by cyclic voltammetry at various scan rates according to a previously reported procedure.^{28,33,51}

The capacitance of SnO₂-Sb/Ti and SnO₂-Sb-Pt/Ti (x = 0.00 at. %) electrodes in alkaline

1
2
3 electrolyte decreases with the potential, showing the characteristic behavior for a n-type
4 semiconductor, whereas that of the RuO₂/Ti electrode increases with the potential, characteristic
5 of p-type semiconductors. The effect of Ru incorporate in SnO₂-Sb(13-x)-Pt-Ru(x)/Ti electrodes
6 is manifested by an increase in capacitance even for low Ru content. These results highlight the
7 marked effect of Ru on the electrochemical response of SnO₂-based electrodes in alkaline
8 conditions.
9

10
11
12
13
14
15
16
17
18
19 The capacitance values provide information on the real, electrochemically-active, surface area of
20 the electrodes through the so-called roughness factor (Rf), which is defined as the real surface
21 area per geometric area of electrode (2 cm²) and is one of the electrocatalytic activity-
22 determining factors. The values of Rf were estimated from the experimental capacitance values
23 at 0.55 V and the specific capacitance of SnO₂-based (8 μF cm⁻²)⁵² and RuO₂ (80 μF cm⁻²)⁵³
24 electrodes. The introduction of Ru (Fig. 9a) produces an increase in the roughness factor at 0.55
25 V and the different voltammetric charges of the SnO₂-Sb(13-x)-Pt-Ru(x)/Ti electrodes, reaching
26 a maximum when x = 3.25 at. %, . Then these parameters slightly decrease with the increase in
27 Ru content.
28
29
30
31
32
33
34
35
36
37
38
39

40
41 The voltammetric charge (q*) is another important parameter influenced by both the real surface
42 area (geometric factors) and the specific electroactivity of the sites, which depends on the
43 chemical composition of the oxide layers (electronic factors). The total (q_{TOT}*), outer (q_{OUT}*)
44 and inner (q_{IN}*) voltammetric charges of the electrodes were measured by using the procedure
45 described in the literature.⁵¹ These charges are related to the total, the most accessible and the
46 less accessible (pores, cracks, grain boundaries, etc.)⁴⁸ electroactive surface, respectively (Fig.
47 9a). These electrical charges show the same tendency as roughness factor. The so-called
48 electrochemical porosity (P_e) (Table 3), obtained from the inner charge to total charge ratio
49
50
51
52
53
54
55
56
57
58
59
60

(q_{IN}^*/q_{TOT}^*) also shows the same tendency.^{28,48} These trends are in good agreement with the morphology changes observed by SEM and suggest that, unlike in acid medium,³³ the electrochemical response of these electrodes in NaOH solution is governed by geometric factors (i.e. by the surface area exposed to the electrolyte solution).

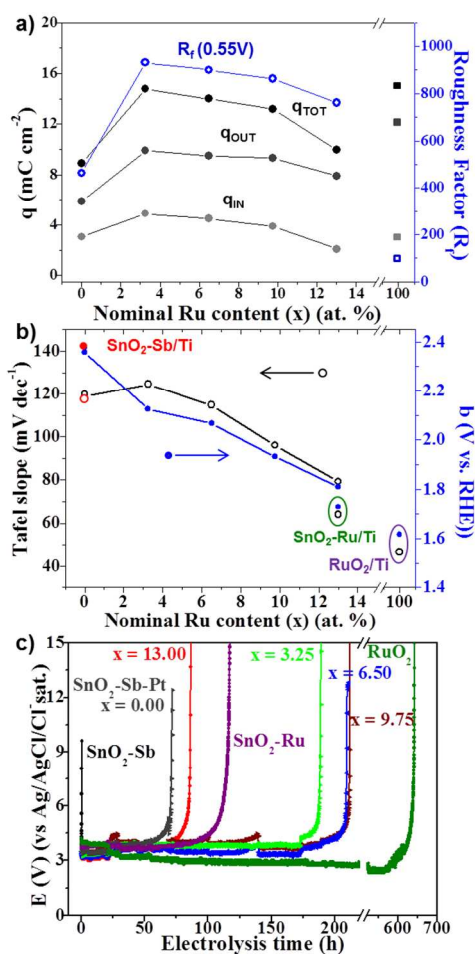


Figure 9. (a) Total (q_{TOT}), outer (q_{OUT}) and inner (q_{IN}) charges and roughness factor for the SnO₂-Sb(13-x)-Pt-Ru(x)/Ti electrodes and RuO₂/Ti electrode as a function of the nominal Ru content; (b) Tafel slope and Tafel line y-intercept as a function of the nominal Ru content; and (c) Potential vs. electrolysis time during service life tests for the different electrodes indicated in the figure.

3.2.2 Oxygen evolution reaction (OER).

The electrocatalytic activity of the different electrodes in alkaline medium was evaluated from the linear region of their corresponding Tafel plots ($\log j$ vs. E)⁵⁴ (see Supp. Info.-Fig. S3). The Tafel slopes provide relevant information on reaction mechanisms, whereas the y-intercept of the Tafel plot at $j = 0$ is related to the exchange current density (j_0), i.e. the intrinsic ability of an electrocatalyst to catalyze a reaction at $\eta = 0$ V.⁵⁴ Thus the lower the y-intercept value (b in Fig. 9b), the higher j_0 . As shown in Fig. 9b, SnO₂-Sb/Ti and SnO₂-Sb-Pt/Ti ($x = 0$) electrodes exhibit a Tafel slope in alkaline conditions of around 120 mV dec⁻¹, which suggests a kinetic control by the adsorption of OH⁻ according to the generally proposed OER mechanism.⁵⁴ These Tafel slopes, together with the high values of y-intercept constant ($b \approx 2.4$ V, Fig. 9b), are in close agreement with those found in the literature for SnO₂-based electrodes^{28,48} and reflect their poor electrocatalytic activity towards the OER. As the Ru content in the oxide layer increases, the values of both constants decrease down to 80 mV dec⁻¹ and 1.8 V, respectively, for $x = 13.0$ at. % electrodes, approaching to those of RuO₂/Ti (~ 40 mV dec⁻¹ and $b \approx 1.6$ V). These low values are typical of RuO₂ anodes and involve the electro-oxidation of the intermediate surface complex as the rate-determining step and a high electrocatalytic activity for the OER in these conditions. Thus, the decrease in Tafel constants indicates that the introduction of Ru in SnO₂-Sb-Pt/Ti electrodes gradually increases the electrocatalytic activity of the electrodes towards the OER, with a weakening of the metal-oxygen bond strength on the surface and a modification of the rate determining step. A similar electrocatalytic effect for Ru in SnO₂-based anodes was also observed by other authors in both acidic^{33,48} and alkaline⁵⁵ media. From Tafel results, it is suggested that the first step becomes more facilitated when Sb is replaced by Ru because of its higher redox activity, the induced change in the charge carrier mechanism, an increase in its

1
2
3 electrical conductivity⁴⁸ and its exceptional ability to form hydrated oxides through the following
4
5 mechanism:⁵¹
6
7



16 3.3 Electrode stability and deactivation mechanism

17 3.3.1 Electrode stability.

18
19
20 Fig. 9c depicts the evolution of the electrode potential with the electrolysis time upon anodic
21 polarization at 0.5 A cm⁻² in 1 M NaOH. The electrode potential remains stable for a certain
22 period of time, the so called service life, until it undergoes a sharp rise indicating deactivation.
23
24 Table 3 summarizes the service life of the different electrodes, expressed as efficiency. The
25 obtained results highlight the extremely short and long service life of the SnO₂-Sb and RuO₂
26 electrodes in 1 M NaOH, respectively. Particularly, the value for SnO₂-Sb is even much shorter
27 than those reported for the deactivation process of Sb-doped SnO₂ electrodes in acidic media.^{21,28}
28
29 By contrast, the stability of RuO₂ in alkaline conditions is much higher than in acid electrolytes
30 (1-3 h).⁵⁶
31
32
33
34
35
36
37
38
39
40
41
42
43
44

45 The introduction of a small amount of Pt (3 at. %) in SnO₂-Sb produces a remarkable stabilizing
46 effect, so that the service life is increased by two orders of magnitude (Table 3). Similar service
47 lives in alkaline medium were observed by Adams et al.,³¹ by introducing Pt in SnO₂-Sb₂O₅
48 electrodes, but using milder anodic polarization conditions (0.16 A cm⁻² and 0.5 M NaOH) and
49 larger Pt contents (PtO_x (10 wt. %)). Nevertheless, the service life of these electrodes in alkaline
50
51
52
53
54
55
56
57
58
59
60

1
2
3 medium is still lower than that in acid conditions, in which Pt was found to cause proportional
4 stabilizing effects.
5
6

7
8
9 The substitution of Sb by Ru in the nominal composition causes an increase in the service life of
10 SnO₂-Sb/Ti and SnO₂-Sb-Pt/Ti electrodes in alkaline conditions. In the presence of Pt, the
11 introduction of Ru increases the service life by up to one order of magnitude for the 9.75 at. %
12 electrode. To the knowledge of the authors, the only study on the stability of binary (Sn-Ru)O₂
13 oxides in alkaline conditions was carried out by Lyons and Burke,⁵⁷ who obtained a maximum
14 service life of 240 h in stronger conditions (6 M NaOH; 0,75 A cm⁻² and 80 °C) for a thicker
15 electrode (4 mg cm⁻²) with 40 % RuO₂. In terms of efficiency, the service life (SLE) of these
16 electrodes (45 Ah mg⁻¹) was considerably lower than those found in this work for Pt- and Ru-
17 doped SnO₂ anodes (63-106 A h mg⁻¹) (Table 3), by using even about 4-12 times higher Ru
18 contents in the former case. The highest stabilities obtained by combining low amounts of Pt (3
19 %) and Ru (3.25-6.50 at. %) highlights the outstanding synergistic effect of Pt and Ru in these
20 quaternary SnO₂-Sb(13-x)-Pt-Ru(x)/Ti mixed oxides. Several strategies have been used in order
21 to improve the service life of these types of electrodes. Recently, the introduction of carbon
22 nanotubes (CNT) in the Ti/SnO₂-Sb-CNT composition increases the service life 4.8 times
23 compared to the Ti/SnO₂-Sb electrode, showing a superior electrochemical oxidation and
24 degradation abilities for organic pollutants³⁰.
25
26
27
28
29
30
31
32
33
34
35
36
37
38
39
40
41
42
43
44
45
46
47

48 3.3.2. Characterization of deactivated electrodes.

49
50

51 Although a little more cracked and deteriorated, the surface texture of the deactivated SnO₂-Sb
52 electrode (Fig. 1b) is rather similar to that of the fresh ones (Fig. 1a), whereas the deactivated
53 SnO₂-Sb-Pt electrode additionally exhibits the detachment of some regions of the oxide coating
54
55
56
57
58
59
60

1
2
3 throughout the whole surface (Fig. 1f) exposing the Ti substrate to the electrolyte (Fig. 1g). In
4
5 RuO₂/Ti electrodes, the anodic polarization process produces the detachment of almost the whole
6
7 RuO₂ layer and only some small fragments remain attached to the support surface after
8
9 deactivation (Fig. 1d). On the other hand, and independently of the Ru content, deactivated
10
11 SnO₂-Sb(13-x)-Pt-Ru(x) /Ti and SnO₂-Ru/Ti electrodes showed a more pronounced detachment
12
13 of the oxide layer than in the case of SnO₂-Sb-Pt/Ti electrode, with small coating fragments but
14
15 less marked than that of RuO₂/Ti. The Sn/M ratio is practically maintained in the deactivated
16
17 electrodes; however, the Sb/M and Ru/M ratios decrease (Table 1), and the Pt/M increases.
18
19
20
21
22

23 The partial detachment of the outer or a localized-region of the SnO₂-based oxide layers was
24
25 evidenced by i) the presence of Sn, Sb and Pt in the used alkaline electrolytes (even in the case of
26
27 SnO₂-Sb), as determined by ICP analysis; ii) the appearance or increase of Ti signal in XPS or
28
29 EDX and XRD results (Fig. S2). In spite of the damage of the outer surface layers, XPS revealed
30
31 that the anodic polarization does not modify the binding energies of Sn(3d), Sb(3d) and O(1s)
32
33 core levels (Fig. 4) of the deactivated electrodes, although metallic Pt completely transforms into
34
35 oxidized Pt (II) and Pt (IV) species (Fig. S1a).⁴³ Moreover, XRD patterns of deactivated
36
37 electrodes still keep the characteristic rutile-like structure.
38
39
40
41
42

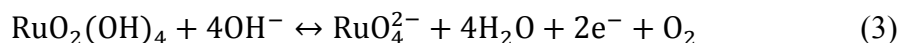
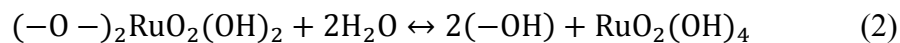
43 The detailed analysis of core level photoelectron spectra of the different deactivated SnO₂-based
44
45 electrodes show a decrease in the I_{OH}/I_{OM} ratios (Table 1), indicating a higher relative increase in
46
47 the amount of oxygen atoms bonded to metal (OM). Moreover, the effect of Ru content in the
48
49 binding energies of Sn 3d_{3/2} and 3d_{5/2} states of the different Ru-doped SnO₂ electrodes,
50
51 disappears after deactivation (Fig. 4b). Also their voltammograms show a dramatic loss of the
52
53 voltammetric charge and do not exhibit the characteristic redox peaks of Ru species within the
54
55
56
57
58
59
60

1
2
3 entire potential range (Fig. 8c-h). The onset of the OER is also shifted to more positive
4 potentials.
5
6

7
8
9 The similarity between the surface Sn/M atomic ratio of fresh and deactivated SnO₂-Sb and
10 SnO₂-Sb-Pt electrodes, determined by XPS (Table 1), together with the general decrease in the
11 corrected I_{OH}/I_{OM} ratios, seem to rule out the formation of a passivating surface layer of tin
12 hydroxides (Sn(OH)₄) and/or hydrates.⁴³ These facts reveal that the deactivation mechanism of
13 these electrodes in alkaline conditions is different to that proposed for acid medium.^{20,26,43} On the
14 other hand, the similar voltammetric profile of fresh and deactivated electrodes (Fig. 8) indicates
15 that the SnO₂-Sb/Ti and SnO₂-Sb-Pt/Ti deactivated ones preserve the ability to transfer charge
16 across the surface. The OER currents are considerably tilted, especially in the case of SnO₂-Sb/Ti
17 electrodes. This fact may be due to the growth of a TiO₂ interlayer.⁵⁸ In the case of SnO₂-Sb-
18 Pt/Ti the conversion of metallic Pt to Pt(IV) and Pt(II) species can originate a reduction in the
19 number of oxygen vacancies⁴² and a decrease of its electrocatalytic activity for OER.
20 Consequently, the deactivation of SnO₂-Sb and SnO₂-Sb-Pt electrodes in NaOH is proposed to
21 occur by a non-selective dissolution of metallic species in alkaline conditions, accompanied by
22 some degree of coating detachment, that allows the NaOH electrolyte to contact and passivate
23 the MO_x/Ti interphase.⁵⁹
24
25
26
27
28
29
30
31
32
33
34
35
36
37
38
39
40
41
42
43
44

45 The detachment of the whole RuO₂ coating in RuO₂/Ti electrodes was confirmed by the
46 remarkably high Ti/M ratio and the increase of both the Ti(2p) core-level peak (associated with
47 TiO₂)⁶⁰ (Fig. S1b) and the relative intensity of Ti diffraction peaks (Fig. S2), as well as the
48 decrease in the Ru(3d) photoelectron peak (Fig. 4d), the complete disappearance of RuO₂
49 diffraction peaks (Fig. S2b) and the absence of Ru redox peaks and extremely low currents in its
50 CV profile (Fig. 8h). This may be related to the electrochemical dissolution of RuO₂ in alkaline
51
52
53
54
55
56
57
58
59
60

1
2
3 medium at high potentials,⁵⁷ which has been associated with the electrochemical generation of
4
5 soluble RuO_4^{2-} species during O_2 production:
6
7



8
9
10
11
12 From the detailed characterization of fresh and deactivated electrodes it is proposed that the
13
14 anodic deactivation of $\text{SnO}_2\text{-Sb}(13\text{-x})\text{-Pt-Ru}(x)/\text{Ti}$ electrodes in NaOH electrolyte, occurs by a
15
16 mixed mechanism. Thus, dissolution of metallic species, promoted in alkaline conditions and
17
18 high potentials, the loss of coating and the passivation of Ti substrate, by formation of an
19
20 insulating TiO_2 interlayer, act together. Considering this mechanism and the service life of the
21
22 different electrodes in NaOH (Table 3), the stabilizing effect of Pt may be attributed to its
23
24 surface compacting effect, what may hinder the penetration of the electrolyte through the
25
26 coating, and/or to prevent the generation of surface insulating $\text{Sn}(\text{OH})_x$ species²⁸ and/or Sb^{3+}
27
28 species, which could be important active sites for oxygen and water adsorption.⁶¹ On the other
29
30 hand, regarding the similarities in microstructure observed by XRD and TEM, the enhanced
31
32 stability caused by the progressive substitution of Sb by Ru up to a 9.75 at. % Ru , at which Sn
33
34 and Ru form a solid solution, together with the decreased stability observed for higher Ru
35
36 contents ($x > 9.75$ at. %), for which a RuO_2 phase segregation is observed, allow us to suggest
37
38 that the formation of a homogeneous $(\text{Ru}_\delta\text{Sn}_{1-\delta})\text{O}_2$ single-phase must be the key factor
39
40 explaining the high stability of $\text{SnO}_2\text{-Sb}(13\text{-x})\text{-Pt-Ru}(x)/\text{Ti}$ electrodes. In addition, the high
41
42 stability of the highest oxidation states of Ru and Pt in alkaline conditions, at potentials where
43
44 the OER occurs, may also contribute. In this sense, the Ru -doped SnO_2 electrodes may
45
46 experience deactivation after the observed selective dissolution of Ru from the $(\text{Ru}_\delta\text{Sn}_{1-\delta})\text{O}_2$
47
48
49
50
51
52
53
54
55
56
57
58
59
60

1
2
3 phase, which may bring about the coating detachment and the access of electrolyte to the Ti
4 support. On the other hand, the segregation of RuO₂ phase may promote the generation of
5 crystalline and structural defects, which could facilitate the dissolution of inner metal species and
6 the penetration of NaOH electrolyte.
7
8
9
10
11

12 13 14 **4. Conclusions** 15

16
17 The introduction of Pt (3 at.%) and the nominal substitution of Sb (13 at.%) by Ru in SnO₂-Sb
18 and SnO₂-Sb-Pt electrodes induce different textural, structural and chemical changes that
19 strongly affect the electrocatalytic activity for the OER and electrochemical stability in alkaline
20 conditions. Although both Pt and Ru are mainly incorporated in the bulk of the SnO₂-Sb(13-x)-
21 Pt-Ru(x) electrodes, they introduce their characteristic redox processes and shift the onset of the
22 OER towards lower potentials. However, while Pt does not alter neither the Sn and Sb contents
23 nor the rutile-like crystalline structure, XPS and XRD analysis have shown that, Ru content
24 lower than 9.75 at. %, Ru(IV) atoms, instead of replacing Sb in the mixed oxides (as it could be
25 expected from the change on nominal compositions), occupy positions of Sn(IV) ions in the
26 cationic sub-lattice of the rutile-like SnO₂ structure to form a solid solution. In addition, surface
27 segregation of Ru is observed as RuO₂ phase at Ru contents larger than 9.75 at.%.
28
29
30
31
32
33
34
35
36
37
38
39
40
41
42
43

44 The deactivation of the different electrodes has been found to occur by passivation of the Ti
45 substrate and/or detachment of the oxide coating promoted by alkaline dissolution of metal
46 species at high potentials. Considering this mechanism, Pt causes a compacting effect on the
47 cracked-mud morphology of the SnO₂-Sb coating that, together with its stability under OER
48 conditions, results an increase in the “accelerated” service life of this electrode by two orders of
49 magnitude in alkaline medium. Moreover, the introduction of low amounts of Ru (3.25-9.75 at.
50
51
52
53
54
55
56
57
58
59
60

1
2
3 %) into the SnO₂ rutile-like structure leads to a three-fold increase in the service life of SnO₂-Sb-
4
5 Pt/Ti electrodes. However, a further gain in stability with higher Ru contents is not observed
6
7 probably because of the mixed metal oxide saturation, which leads to Ru segregation as a RuO₂
8
9 phase.
10

11
12
13
14 Consequently, the obtained results show that the combination of low amounts of Pt and Ru
15
16 (below the saturation of (Ru_δSn_{1-δ})O₂ solid solutions) greatly enhances the stability of SnO₂-Sb
17
18 electrodes in alkaline medium. Although the stability of these electrodes does not reach that
19
20 observed for pure RuO₂, they constitute cheaper alternatives with a higher OER overpotential as
21
22 attractive properties for different applications in alkaline medium, such as electro-oxidation of
23
24 compounds in electrosynthesis and electrochemical degradation of pollutants.
25
26
27

28 29 ASSOCIATED CONTENT

30 31 **Supporting Information**

32
33
34 Additional XPS, XRD and Tafel plots information. This material is available free of charge via
35
36 the Internet at <http://pubs.acs.org>.
37
38

39 40 AUTHOR INFORMATION

41 42 **Corresponding Author**

43
44
45 *Email: morallon@ua.es.
46
47

48 49 ACKNOWLEDGEMENTS

50
51 The authors thanks to the MINECO, FEDER and Generalitat Valenciana for the financial support
52
53 (MAT2013-42007-P, PROMETEO2013/028 projects).
54
55

56 57 REFERENCES

1
2
3 (1) Trasatti, S. Transition Metal Oxides: Versatile Materials for Electrocatalysis. In *The*
4 *Electrochemistry of Novel Materials*; Lipkowski, J.; Ross, P. N., Eds.; VCH Publisher Inc.;
5
6 Weinheim, 1994, pp 207–295.
7
8

9
10
11 (2) Hayfield, P. C. S. Development of the Noble Metal/Oxide Coated Titanium Electrode Part
12 III: Coated Titanium Anodes in Widely Ranging Oxygen Evolving Situations. *Platinum Met.*
13 *Rev.* **1998**, 42, 116–122.
14
15
16

17
18
19 (3) Park, S.; Shao, Y.; Liu, J.; Wang, Y. Oxygen Electrocatalysts for Water Electrolyzers and
20 Reversible Fuel Cells: Status and Perspective. *Energy Environ. Sci.* **2012**, 5, 9331–9344.
21
22
23

24
25 (4) McCrory, C. C. L.; Jung, S.; Peters, J. C.; Jaramillo, T. F. Benchmarking Heterogeneous
26 Electrocatalysts for the Oxygen Evolution Reaction. *J. Am. Chem. Soc.* **2013**, 135, 16977–16987.
27
28
29

30
31 (5) Martínez-Huitle, C. A.; Ferro, S. Electrochemical Oxidation of Organic Pollutants for the
32 Wastewater Treatment: Direct and Indirect Processes. *Chem. Soc. Rev.* **2006**, 35, 1324–1340.
33
34
35

36 (6) Comninellis, Ch.; Pulgarin, C. Anodic Oxidation of Phenol for Waste-Water Treatment. *J.*
37 *Appl. Electrochem.* **1991**, 21, 703–708.
38
39
40

41 (7) Chen, G.; Hung, Y. T. Electrochemical Wastewater Treatment Processes. In *Advanced*
42 *Physicochemical Treatment Technologies*; Wang, L. K.; Hung, Y. T.; Shammass, N. K., Eds.;
43
44 Handbook of Environmental Engineering Series 5, Springer-Verlag; New York, LLC, 2007; pp
45
46 57–106.
47
48
49

50
51 (8) Berenguer, R.; Marco-Lozar, J. P.; Quijada, C.; Cazorla-Amorós, D.; Morallón, E.
52 Electrochemical Regeneration and Porosity Recovery of Phenol-saturated Granular Activated
53
54 Carbon in an Alkaline Medium. *Carbon* **2010**, 48, 2734–2745.
55
56
57
58
59
60

1
2
3 (9) Berenguer, R.; Marco-Lozar, J. P.; Quijada, C.; Cazorla-Amorós, D.; Morallón, E.
4
5 Comparison among Chemical, Thermal, and Electrochemical Regeneration of Phenol-Saturated
6
7 Activated Carbon. *Energy Fuels* **2010**, 24, 3366–3372.
8
9

10
11 (10) Lin, H.; Niu, J.; Ding, S.; Zhang, L. Electrochemical Degradation of Perfluorooctanoic
12
13 Acid (PFOA) by Ti/SnO₂-Sb, Ti/SnO₂-Sb/PbO₂ and Ti/SnO₂-Sb/MnO₂ Anodes. *Water Res.*
14
15 **2012**, 46, 2281-2289.
16
17

18
19 (11) Lin, H.; Niu, J.; Xu, J.; Huang, H.; Li, D.; Yue, Z.; Feng, C. Highly Efficient and Mild
20
21 Electrochemical Mineralization of Long-Chain Perfluorocarboxylic Acids (C₉–C₁₀) by
22
23 Ti/SnO₂-Sb-Ce, Ti/SnO₂-Sb/Ce-PbO₂, and Ti/BDD Electrodes. *Environ. Sci. Technol.* **2013**,
24
25 47, 13039-13046.
26
27

28
29 (12) Niu, J.; Bao, Y.; Li, Y.; Chai, Z. Electrochemical Mineralization of Pentachlorophenol
30
31 (PCP) by Ti/SnO₂-Sb Electrodes. *Chemosphere* **2013**, 92, 1571-1577.
32
33

34
35 (13) Simon, P.; Gogotsi, Y. Materials for Electrochemical Capacitors. *Nat. Mater.* **2008**, 7,
36
37 845–854.
38
39

40
41 (14) Wang, G.; Zhang, L.; Zhang, J. A Review of Electrode Materials for Electrochemical
42
43 Supercapacitors. *Chem. Soc. Rev.* **2012**, 41, 797–828.
44
45

46
47 (15) Sieben, J. M.; Morallón, E.; Cazorla-Amorós, D. Flexible Ruthenium Oxide-Activated
48
49 Carbon Cloth Composites Prepared by Simple Electrodeposition Methods. *Energy* **2013**, 58,
50
51 519–526.
52
53

54
55 (16) Tarascon, J. M.; Armand, M. Issues and Challenges Facing Rechargeable Lithium
56
57 Batteries. *Nature* **2001**, 414, 359–367.
58
59
60

1
2
3 (17) Trasatti, S. Electrocatalysis: Understanding the Success of DSA®. *Electrochim. Acta*
4
5 **2000**, 45, 2377–2385.

6
7
8
9 (18) Vercesi, G. P.; Rolewicz, J.; Comninellis, Ch.; Hinden, J. Characterization of DSA-Type
10
11 Oxygen Evolving Electrodes. Choice of Base Metal. *Thermochim. Acta* **1991**, 176, 31–47.

12
13
14 (19) Comninellis, Ch.; Vercesi, G. P. Characterization of DSA-Type Oxygen Evolving
15
16 Electrodes. Choice of a Coating. *J. Appl. Electrochem.* **1991**, 21, 335–345.

17
18
19
20 (20) Stucki, S.; Kotz, R.; Carcer, B.; Suter, W. Electrochemical Waste-Water Treatment using
21
22 High Overvoltage Anodes. 2. Anode Performance and Applications. *J. Appl. Electrochem.* **1991**,
23
24 21, 99–104.

25
26
27
28 (21) Correa-Lozano, B.; Comninellis, Ch.; De Battisti, A. Service Life of Ti/SnO₂-Sb₂O₅
29
30 Anodes. *J. Appl. Electrochem.* **1997**, 27, 970–974.

31
32
33 (22) Rodgers, J.D.; Jedral, W. J.; Bunce, N.J. Electrochemical Oxidation of Chlorinated
34
35 Phenols. *Environ. Sci. Technol.* **1999**, 33, 1453–1457.

36
37
38
39 (23) Cañizares, P.; Martínez, F.; Díaz, M.; García-Gómez, J.; Rodrigo, M. A. Electrochemical
40
41 Oxidation of Aqueous Phenol Wastes Using Active and Nonactive Electrodes. *J. Electrochem.*
42
43 *Soc.* **2002**, 149, D118–D124.

44
45
46
47 (24) Montilla, F.; Michaud, P. A.; Morallón, E.; Vázquez, J. L.; Comninellis, Ch.;
48
49 Electrochemical Oxidation of Benzoic Acid at Boron-Doped Diamond Electrodes. *Electrochim.*
50
51 *Acta* **2002**, 47, 3509–3513.

52
53
54
55 (25) Treimer, S. E.; Feng, J.; Scholten, M. D.; Johnson, D. C.; Davenport, A. J. Comparison of
56
57 Voltammetric Responses of Toluene and Xylenes at Iron(III)-Doped, Bismuth(V)-Doped, and
58
59
60

1
2
3 Undoped Beta-Lead Dioxide Film Electrodes in 0.50 M H₂SO₄. *J. Electrochem. Soc.* **2001**, 148,
4 E459–E463.
5
6

7
8
9 (26) Vicent, F.; Morallon, E.; Quijada, C.; Vazquez, J. L.; Aldaz, A.; Cases, F.
10 Characterization and Stability of Doped SnO₂ Anodes. *J. Appl. Electrochem.* **1998**, 28, 607–612.
11
12

13
14 (27) Ding, H. Y.; Feng, Y. J.; Lu, J. W. Study on the Service Life and Deactivation Mechanism
15 of Ti/SnO₂-Sb Electrode by Physical and Electrochemical Methods. *Russ. J. Electrochem.* **2010**,
16 46, 72–76.
17
18

19
20
21 (28) Montilla, F.; Morallón, E.; De Battisti, A.; Vázquez, J. L. Preparation and
22 Characterization of Antimony-Doped Tin Dioxide Electrodes. Part 1. Electrochemical
23 Characterization. *J. Phys. Chem. B* **2004**, 108, 5036–5043.
24
25
26

27
28 (29) Forti, J. C.; Olivi, P.; de Andrade, A. R. Characterisation of DSA®-Type Coatings with
29 Nominal Composition Ti/Ru_{0.3}Ti_(0.7-x)Sn_xO₂ Prepared Via a Polymeric Precursor. *Electrochim.*
30 *Acta* **2001**, 47, 913–920.
31
32
33

34
35 (30) Zhang, L.; Xu, L.; He, J.; Zhang, J. Preparation of Ti/SnO₂-Sb Electrodes Modified by
36 Carbon Nanotube for Anodic Oxidation of Dye Wastewater and Combination with
37 Nanofiltration. *Electrochim. Acta* **2014**, 117, 192-201.
38
39
40
41

42
43 (31) Adams, B.; Tian, M.; Chen, A. Design and Electrochemical Study of SnO₂-based Mixed
44 Oxide Electrodes. *Electrochim. Acta* **2009**, 54, 1491–1498.
45
46
47

48
49 (32) Montilla, F.; Morallón, E.; Vázquez, J. L. Evaluation of the Electrocatalytic Activity of
50 Antimony-Doped Tin Dioxide Anodes Toward the Oxidation of Phenol in Aqueous Solutions. *J.*
51 *Electrochem. Soc.* **2005**, 152, B421–B427.
52
53
54
55
56
57
58
59
60

1
2
3 (33) Berenguer, R.; Quijada, C.; Morallón, E. Electrochemical Characterization of SnO₂
4 Electrodes Doped with Ru and Pt. *Electrochim. Acta* **2009**, 54, 5230–5238.
5
6

7
8 (34) Iwakura, C.; Sakamoto, K. Effect of Active Layer Composition on the Service Life of
9 (SnO₂ and RuO₂)-Coated Ti Electrodes in Sulfuric-Acid Solution. *J. Electrochem. Soc.* **1985**,
10 132, 2420–2423.
11
12
13

14
15 (35) Fachinotti, E.; Guerrini, E.; Tavares, A.C.; Trasatti, S. Electrocatalysis of H₂ Evolution
16 by Thermally Prepared Ruthenium Oxide: Effect of Precursors: Nitrate vs. Chloride. *J.*
17 *Electroanal. Chem.* **2007**, 600, 103–112.
18
19
20
21
22

23
24 (36) De Pauli, C. P.; Trasatti, S. Electrochemical Surface Characterization of IrO₂+SnO₂
25 Mixed-Oxide Electrocatalysts. *J. Electroanal. Chem.* **1995**, 396, 161–168.
26
27
28

29
30 (37) Matko, I.; Gaidi, M.; Chenevier, B.; Charai, A.; Saikaly, W.; Labeau, M. Pt Doping of
31 SnO₂ Thin Films: A Transmission Electron Microscopy Analysis of the Porosity Evolution. *J.*
32 *Electrochem. Soc.* **2002**, 149, H153–H158.
33
34
35
36

37
38 (38) Ito, M.; Murakami, Y.; Kaji, H.; Yohikozawa, K.; Takasu, Y. Surface Characterization of
39 RuO₂-SnO₂ Coated Titanium Electrodes. *J. Electrochem. Soc.* **1996**, 143, 32–36.
40
41
42

43
44 (39) Nanni, L.; Polizzi, S.; Benedetti, A.; De Battisti, A. Morphology, Microstructure, and
45 Electrochemical Properties of RuO₂-SnO₂ Thin Films. *J. Electrochem. Soc.* **1999**, 146, 220–225.
46
47
48

49
50 (40) Wang, X.; Deng, F.; Tang, Z.; Wu, B.; Tang, D.; Lin, W. The Nature of Phase Separation
51 in a Ru-Sn-O Ternary Oxide Electrocatalyst. *Phys. Chem. Chem. Phys.* **2013**, 15, 3977–3984.
52
53
54

55
56 (41) Liu, W.; Cao, X.; Zhu, Y.; Cao, L. The Effect of Dopants on the Electronic Structure of
57 SnO₂ Thin Film. *Sens. Actuators, B* **2000**, 66, 219–221.
58
59
60

1
2
3 (42) Batzill, M.; Diebold, U. The Surface and Materials Science of Tin Oxide. *Prog. Surf. Sci.*
4
5 **2005**, 79, 47–154.
6

7
8 (43) Montilla, F.; Morallón, E.; De Battisti, A.; Barison, S.; Daolio, S.; Vázquez, J. L.
9 Preparation and Characterization of Antimony-Doped Tin Dioxide Electrodes. 3. XPS and SIMS
10 Characterization. *J. Phys. Chem. B* **2004**, 108, 15976–15981.
11
12
13

14 (44) Montilla, F.; Morallón, E.; De Battisti, A.; Benedetti, A.; Yamashita, H.; Vázquez, J. L.
15 Preparation and Characterization of Antimony-Doped Tin Dioxide Electrodes. Part 2. XRD and
16 EXAFS Characterization. *J. Phys. Chem. B* **2004**, 108, 5044–5050.
17
18
19

20 (45) Terrier, C.; Chatelon, J. P.; Roger, J. A.; Berjoan, R.; Dubois, C. Analysis of Antimony
21 Doping in Tin Oxide Thin Films Obtained by the Sol-Gel Method. *J. Sol-Gel Sci. Technol.* **1997**,
22 10, 75–81.
23
24

25 (46) Slater, B.; Catlow, C. R.; Gay, D. H.; Williams, D. E.; Dusastre, V. Study of Surface
26 Segregation of Antimony on SnO₂ Surfaces by Computer Simulation Techniques. *J. Phys. Chem.*
27 *B* **1999**, 103, 10644–10650.
28
29

30 (47) Rochefort, D.; Daboa, P.; Guay, D.; Sherwood, P. M. A. XPS Investigations of Thermally
31 Prepared RuO₂ Electrodes in Reductive Conditions. *Electrochim. Acta* **2003**, 48, 4245–4252.
32
33
34

35 (48) Gaudet, J.; Tavares, A. C.; Trasatti, S.; Guay, D. Physicochemical Characterization of
36 Mixed RuO₂-SnO₂ Solid Solutions. *Chem. Mater.* **2005**, 17, 1570–1579.
37
38
39

40 (49) Berenguer, R.; Valdés-Solís, T.; Fuertes, A. B.; Quijada, C.; Morallón, E. Cyanide and
41 Phenol Oxidation on Nanostructured Co₃O₄ Electrodes Prepared by Different Methods. *J.*
42 *Electrochem. Soc.* **2008**, 155, K110–K115.
43
44
45
46
47
48
49
50
51
52
53
54
55
56
57
58
59
60

1
2
3 (50) Kim, K. W.; Lee, E. H.; Kim, J. S.; Shin, K. H.; Kim, K. H. Study on the Electroactivity
4 and Non-Stoichiometry of a Ru-based Mixed Oxide Electrode. *Electrochim. Acta* **2001**, 46, 915–
5
6 921.
7
8

9
10
11 (51) Ardizzone, S.; Fregonara, G.; Trasatti, S. Inner and Outer Active Surface of RuO₂
12 Electrodes. *Electrochim. Acta* **1990**, 35, 263–267.
13
14

15
16
17 (52) Wu, N. L.; Hwang, J. Y.; Liu, P. Y.; Han, C. Y.; Kuo, S. L.; Liao, K. H.; Lee, M. H.;
18 Wang, S. Y. Synthesis and Characterization of Sb-Doped SnO₂ Xerogel Electrochemical
19 Capacitor. *J. Electrochem. Soc.* **2001**, 148, A550–A553.
20
21
22

23
24
25 (53) Sugimoto, W.; Kizaki, T.; Yokoshima, K.; Murakami, Y.; Takasu, Y. Evaluation of the
26 Pseudocapacitance in RuO₂ with a RuO₂/GC Thin Film Electrode. *Electrochim. Acta* **2004**, 49,
27 313–320.
28
29
30

31
32
33 (54) Bard, A. J.; Faulkner, L. R. *Electrochemical Methods* 1980, John Wiley & Sons: New
34 York.
35
36

37
38 (55) Consonni, V.; Trasatti, S.; Pollak, F.; O'Grady, W. E. Mechanism of Chlorine Evolution
39 on Oxide Anodes. Study of pH Effects. *J. Electroanal. Chem.* **1987**, 228, 393–406.
40
41
42

43
44 (56) Mattos-Costa, F. I.; de Lima-Neto, P.; Machado, S. A. S.; Avaca, L. A. Characterisation
45 of Surfaces Modified by Sol-Gel Derived Ru_xIr_{1-x}O₂ Coatings for Oxygen Evolution in Acid
46 Medium. *Electrochim. Acta* **1998**, 44, 1515–1523.
47
48
49

50
51
52 (57) Lyons, M. E. G.; Burke, L. D. Mechanism of Oxygen Reactions at Porous Oxide
53 Electrodes. 1. Oxygen Evolution at RuO₂ and Ru_xSn_{1-x}O₂ Electrodes in Alkaline-Solution under
54 Vigorous Electrolysis Conditions. *J. Chem. Soc., Faraday Trans. 1* **1987**, 83, 299–321.
55
56
57
58
59
60

1
2
3 (58) Boodts, J. F. C.; Trasatti, S. Effect of Composition on the Electrocatalytic Activity of the
4 Ternary Oxide $\text{Ru}_{0.3}\text{Ti}_{0.7-x}\text{Sn}_x\text{O}_2$. 1. Oxygen Evolution from HClO_4 Solution. *J. Electrochem.*
5
6
7
8 *Soc.* **1990**, 137, 3784–3789.
9

10
11 (59) Beck, F. Wear Mechanisms of Anodes. *Electrochim. Acta* **1989**, 34, 811–822.
12

13
14 (60) Hopfengärtner, G.; Borgmann, D.; Rademacher, I.; Wedler, G.; Hums, E.; Spitznagel, G.
15
16
17 W. XPS Studies of Oxidic Model Catalysts: Internal Standards and Oxidation Numbers. *J.*
18
19 *Electron Spectros. Relat. Phenom.* **1993**, 63, 91–116.
20

21
22 (61) Dusastre, V.; Williams, D. E. Sb(III) as a Surface Site for Water Adsorption on $\text{Sn}(\text{Sb})\text{O}_2$,
23
24 and its Effect on Catalytic Activity and Sensor Behavior. *J. Phys. Chem. B* **1998**, 102, 6732–
25
26
27 6737.
28
29
30
31
32
33
34
35
36
37
38
39
40
41
42
43
44
45
46
47
48
49
50
51
52
53
54
55
56
57
58
59
60

